LETTER

doi:10.1038/nature20168

Designer matrices for intestinal stem cell and organoid culture

Nikolce Gjorevski[1], Norman Sachs[2], Andrea Manfrin[1], Sonja Giger[1], Maiia E. Bragina[1], Paloma Ordóñez-Morán[3], Hans Clevers[2] & Matthias P. Lutolf[1,4]

Epithelial organoids recapitulate multiple aspects of real organs, making them promising models of organ development, function and disease[1–3]. However, the full potential of organoids in research and therapy has remained unrealized, owing to the poorly defined animal-derived matrices in which they are grown[4]. Here we used modular synthetic hydrogel networks[5,6] to define the key extracellular matrix (ECM) parameters that govern intestinal stem cell (ISC) expansion and organoid formation, and show that separate stages of the process require different mechanical environments and ECM components. In particular, fibronectin-based adhesion was sufficient for ISC survival and proliferation. High matrix stiffness significantly enhanced ISC expansion through a yes-associated protein 1 (YAP)-dependent mechanism. ISC differentiation and organoid formation, on the other hand, required a soft matrix and laminin-based adhesion. We used these insights to build a fully defined culture system for the expansion of mouse and human ISCs. We also produced mechanically dynamic matrices that were initially optimal for ISC expansion and subsequently permissive to differentiation and intestinal organoid formation, thus creating well-defined alternatives to animal-derived matrices for the culture of mouse and human stem-cell-derived organoids. Our approach overcomes multiple limitations of current organoid cultures and greatly expands their applicability in basic and clinical research. The principles presented here can be extended to identify designer matrices that are optimal for long-term culture of other types of stem cells and organoids.

Organoids formed by self-organizing stem cells resemble their native counterparts in cellular content, multicellular architecture and functional features. As such, they are emerging as powerful tools in basic and translational research. Intestinal organoids possess a particularly high level of multicellular organization and a wide range of potential applications[7]. When cultured under the appropriate 3D conditions, single Lgr5-expressing ISCs undergo cycles of self-renewal, differentiation and morphogenesis, and self-organize into crypt–villus domains that house both cycling ISCs and differentiated intestinal cells[8]. These organoids hold promise as models of the ISC niche, intestinal development and function[7], as models of patient-specific epithelial diseases[9], and as sources of tissue for autologous transplants[10].

Current organoid culture methods are complicated by the nearly exclusive dependence on animal-derived hydrogels, including Matrigel[11] and collagen[12], as the 3D matrix. These matrices feature complex and variable compositions[13,14], are not conducive to controlled modifications and pose risks of immunogen and pathogen transfer, which makes them unsuitable for organoid expansion with downstream clinical applications. Synthetic ECM analogues are promising alternatives to native matrices[5,15]. Biochemical and biophysical components can be varied, and their influence on biological processes can be tested systematically, allowing for the identification of cellular-system-specific 3D culture environments. Here we used synthetic ECMs to define the microenvironmental parameters that govern ISC behaviour and intestinal organoid formation. We used this insight to create a well-defined 3D matrix for the culture of ISCs and intestinal organoids.

To assess whether a 3D gel matrix is sufficient for ISC expansion and organoid formation, we embedded single dissociated mouse ISCs into enzymatically crosslinked polyethylene glycol (PEG) hydrogels[16], which are soft and hydrated, thus mimicking the basic physical properties of Matrigel without contributing any biochemical signals. Whereas cells cultured in Matrigel divided to form lumen-containing colonies (Extended Data Fig. 1a), those embedded in soft (~300 Pa) PEG gels did not (Fig. 1a), suggesting that not only the physical support in 3D, but also biochemical signals produced by the matrix are required for ISC survival and proliferation. Indeed, enrichment of our inert PEG gels with fibronectin, laminin-111, collagen IV, hyaluronic acid and perlecan, key ECM components located at the bottom of the crypts *in vivo*[17–21], enhanced ISC survival and proliferation (Fig. 1a, b).

Aiming to create the most minimal, chemically defined environment, we replaced full-length fibronectin with an RGD (Arg-Gly-Asp) peptide. Like fibronectin, RGD stimulated ISC colony formation in a concentration-dependent fashion (Fig. 1c, d). Freshly isolated mouse intestinal crypts embedded in RGD-functionalized PEG gels (PEG RGD) likewise survived and formed expanding colonies (Extended Data Fig. 1b). Cells maintained in PEG RGD preserved their colony formation efficiency and Lgr5 expression after at least four passages, indicating that single ISCs can be successfully expanded within PEG RGD gels (Fig. 1e, f) without losing their organoid formation capacity, once re-embedded in Matrigel (Fig. 1g, h). Quantitative reverse transcription polymerase chain reaction (qRT–PCR) confirmed that, under ISC expansion conditions, Lgr5 was highly expressed in both PEG RGD and Matrigel (Extended Data Fig. 1c). As expected, markers of differentiated intestinal cell types became upregulated under organoid formation conditions. Notably, lysozyme appeared to be significantly expressed in Matrigel-based ISC expansion culture, indicating that colonies expanded in Matrigel contain a population of differentiated Paneth cells, which were notably absent in the PEG gels (Extended Data Fig. 1d). Hence, minimal PEG-based matrices may be more suitable for the maintenance of a pure $Lgr5^+$ ISC population.

Embryonic and adult stem cells, including ISCs, are influenced by their mechanical environment[22,23]. We increased our understanding of the mechanical regulation of ISCs by considering the effects of matrix stiffness, which have not been examined before, as performing controlled mechanical modulations *in vivo* and in Matrigel is challenging. In the presence of 1 mM RGD, matrix stiffness indeed influenced ISC colony formation (Fig. 2a, b, Extended Data Fig. 1e): ISC expansion was optimal within matrices of intermediate stiffness (1.3 kPa), whereas stem cells embedded in soft matrices (300 Pa) proliferated poorly. ISC expansion in stiff matrices required cytoskeletal tension

[1]Laboratory of Stem Cell Bioengineering, Institute of Bioengineering, School of Life Sciences (SV) and School of Engineering (STI), Ecole Polytechnique Fédérale de Lausanne (EPFL), Lausanne, Switzerland. [2]Hubrecht Institute and University Medical Center Utrecht, Uppsalalaan 8, 3584CT Utrecht, The Netherlands. [3]Swiss Institute for Experimental Cancer Research (ISREC), EPFL, Lausanne, Switzerland. [4]Institute of Chemical Sciences and Engineering, School of Basic Science, Ecole Polytechnique Fédérale de Lausanne (EPFL), Lausanne, Switzerland.

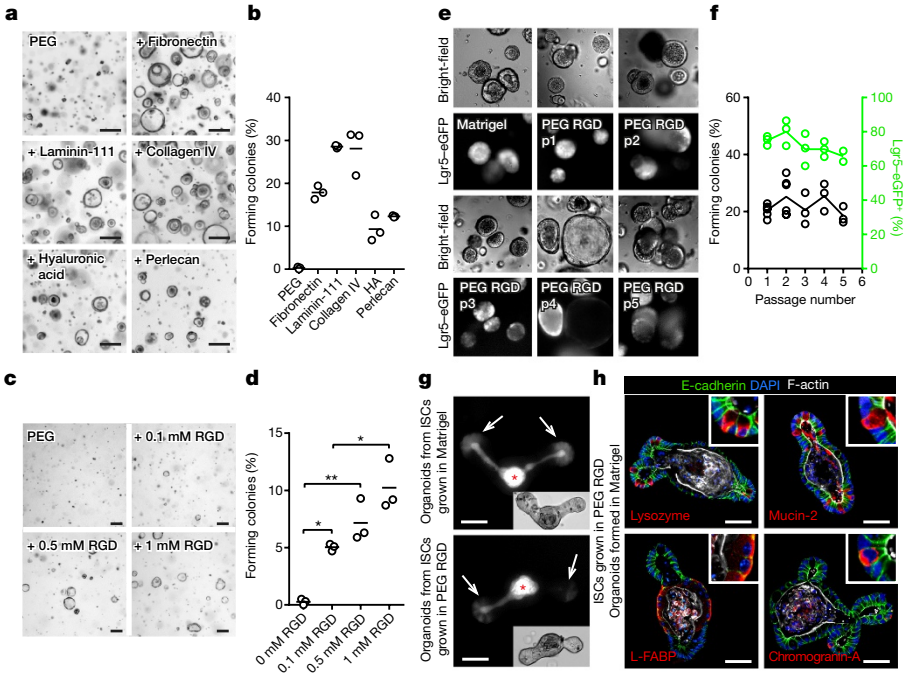

Figure 1 | Building a synthetic ISC niche. a, Mouse ISCs embedded in plain PEG and PEG functionalized with the indicated ECM components. **b**, Quantification of colony formation efficiency. HA, hyaluronic acid. **c**, **d**, Effect of RGD concentration on ISC colony formation in PEG (**c**) and quantification (**d**). **e**, **f**, ISC colony formation in Matrigel and PEG RGD (**e**) and quantification (**f**). **g**, Organoids formed from ISC colonies expanded in Matrigel and PEG RGD. Asterisks indicate autofluorescence. Arrows indicate Lgr5-expressing ISCs. **h**, Organoids formed from ISC colonies expanded in PEG RGD and then transplanted into Matrigel contain differentiated intestinal cells. Graphs show individual data points derived from $n = 3$ independent experiments and means. $^{*}P < 0.05$; $^{**}P < 0.01$; $^{***}P < 0.01$. Scale bars, 50 μm.

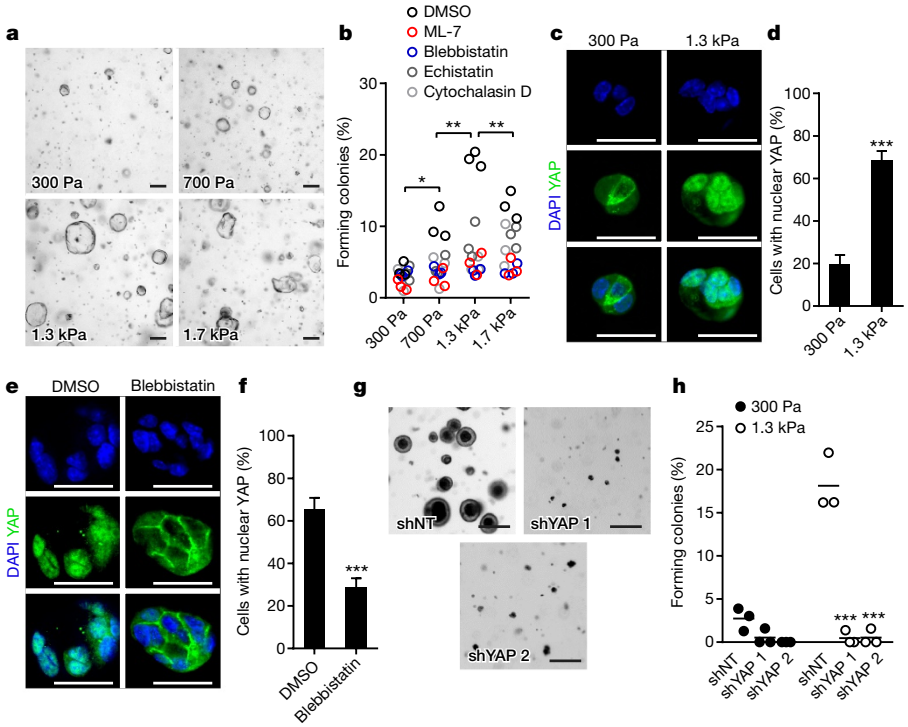

Figure 2 | Matrix mechanical properties control ISC proliferation. a, ISC colony formation in PEG RGD hydrogels of varying stiffness. **b**, Effect of matrix stiffness, cellular contractility and adhesion on ISC colony formation. Graphs show individual data points derived from $n = 3$ independent experiments and means. **c**, **d**, Distribution of YAP in day 1 ISC colonies (**c**) and quantification (**d**). $n = 27$ colonies (300 kPa) and $n = 21$ (1.3 kPa). Data are represented as mean ± s.e.m. **e**, **f**, Distribution of YAP in day 1 colonies formed in 1.3 kPa matrices treated with DMSO or blebbistatin (**e**) and quantification (**f**). $n = 27$ colonies (DMSO) and $n = 30$ (blebbistatin). Data are represented as mean ± s.e.m. **g**, Effect of YAP knockdown on ISC colony formation (**g**) and quantification (**h**). Graphs show individual data points derived from $n = 3$ independent experiments and means. $^{*}P < 0.05$; $^{**}P < 0.01$; $^{***}P < 0.01$. Scale bars, 50 μm.

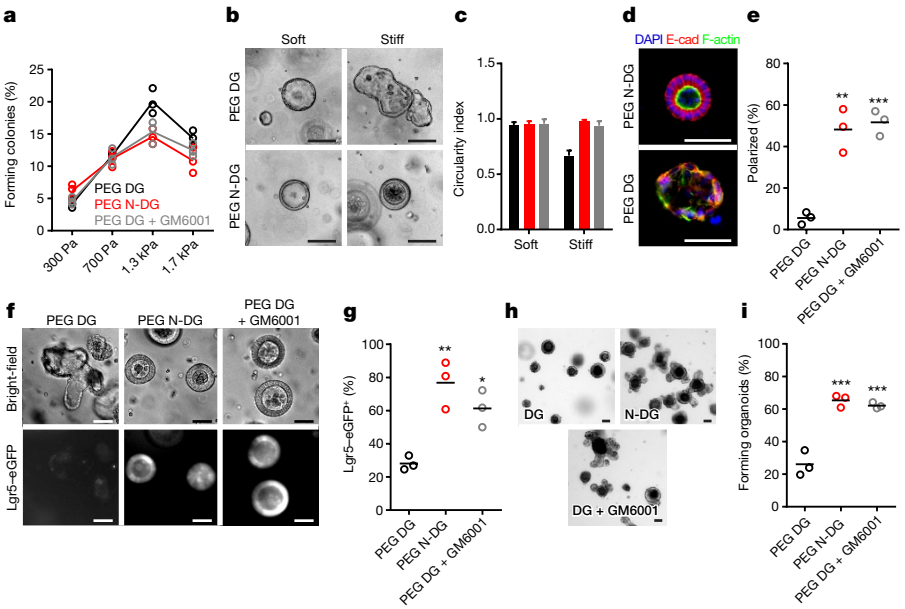

Figure 3 | ISC proteolytic activity influences proliferation, morphology and fate. a, Colony formation efficiency of ISCs embedded in degradable (DG) or non-degradable (N-DG) PEG gels of varying stiffness. **b**, **c**, The effect of matrix degradability on ISC colony shape (**b**) and quantification (**c**). Data are represented as mean ± s.d. Number of colonies analysed was 13 (soft PEG DG), 25 (stiff PEG DG), 5 (soft PEG N-DG), 5 (stiff PEG N-DG), 7 (soft PEG DG + GM6001) and 8 (stiff PEG DG + GM6001). **d**, Colonies in PEG DG and PEG N-DG, stained for F-actin and E-cadherin. **e**, Quantification of the percentage of columnar and polarized colonies. **f**, **g**, Lgr5–eGFP expression within colonies cultured in PEG DG and PEG N-DG (**f**) and quantification (**g**). **h**, **i**, Organoid formation from ISC colonies expanded in PEG DG or PEG N-DG and transferred to Matrigel (**h**) and quantification (**i**). Individual data points derived from $n = 3$ independent experiments and means are shown (**a**, **e**, **g**, **i**). $^{*}P < 0.05$; $^{**}P < 0.01$; $^{***}P < 0.01$. Scale bars, 50 μm.

and integrin-based adhesion, as pharmacological blocking of cell contractility and integrin binding reduced colony formation (Fig. 2b).

YAP, an effector of the Hippo signalling pathway, is crucial for ISC self-renewal and expansion during intestinal tissue regeneration and organoid formation *in vitro*[24,25]. In addition, YAP has been implicated in cellular mechanosensing and mechanotransduction, displaying enhanced nuclear translocation and activation in response to mechanical tension[26,27]. To test whether YAP mediates the mechanical dependence of ISC expansion, we assessed its subcellular localization within colonies grown in soft matrices compared to stiff matrices. Whereas colonies in soft matrices featured predominantly cytoplasmic localization, YAP was highly nuclear within cells grown in stiff matrices (Fig. 2c, d). Pharmacological dissipation of mechanical tension led to a significant reduction in the nuclear translocation of YAP in stiff matrices (Fig. 2e, f). Likewise, controlled matrix softening (Extended Data Fig. 2a) resulted in a change in colony morphology (Extended Data Fig. 2b), cytoplasmic translocation of YAP within 4–8 h (Extended Data Fig. 2c, d), and growth arrest (Extended Data Fig. 2e). Depletion of YAP, using lentiviral delivery of short hairpin RNA (shRNA) (Extended Data Fig. 2f), led to a marked reduction in ISC colony formation within PEG hydrogels (Fig. 2g, h), as did blocking YAP activity with the small molecule verteporfin (Extended Data Fig. 2g), which suggests that YAP activity is required for ISC expansion within PEG matrices. Collectively, these data suggest that matrix stiffness controls ISC expansion by influencing YAP activity.

Noting that proteolytic remodelling is important for morphogenesis and repair[28], we reasoned that making the PEG RGD gels susceptible to degradation by matrix metalloproteinases would render them more physiological, and potentially enhance ISC growth. Therefore, a mutated collagen-I-derived sequence[16], which can be rapidly cleaved by cell-secreted matrix metalloproteinases, was incorporated in the backbone of the polymer network. Although conferring degradability enhanced ISC colony formation in stiff matrices (Fig. 3a), the resulting colonies adopted irregular shapes (Fig. 3b, c), were depolarized and disorganized (Fig. 3d, e), and had attenuated Lgr5 expression (Fig. 3f, g) and organoid formation capacity (Fig. 3h, i). RNA sequencing and gene set enrichment analysis revealed significant upregulation of stress and inflammation signalling-related genes within degradable matrices (Extended Data Fig. 3, Extended Data Tables 2 and 3; GEO, GSE85391). Hence, by enabling ISCs cultured within a stiff environment to engage in rapid matrix degradation, we modelled a pathological, inflammation-like state, that appears to be deleterious to stem cell maintenance.

Next, to test whether PEG RGD gels optimized for ISC expansion also support differentiation and organoid formation, we switched expanded colonies derived from Lgr5–eGFP–ires–CreERT2 mouse intestinal crypts to differentiation conditions, which led to global loss of Lgr5–eGFP and colony destruction in both degradable and non-degradable PEG RGD gels (Extended Data Fig. 4a). To shed light on the deficiencies blocking organoid formation within PEG RGD, we monitored differentiating ISC colonies in both PEG RGD and Matrigel by time-lapse imaging. In Matrigel, we observed attenuation in Lgr5 expression within 24 h (Extended Data Fig. 4b). Faint Lgr5–eGFP expression was detected at punctate locations, which formed buds by 48 h; the Lgr5–eGFP signal was then recovered in the newly formed buds. In synthetic matrices, the initial steps paralleled those in Matrigel. However, instead of forming external buds, the Lgr5–eGFP epithelial patches thickened and buckled (Extended Data Fig. 4b). Comparing the temporal profiles of YAP localization within PEG and Matrigel, we found that, within stiff matrices, the proportion of cells with nuclear YAP sharply dropped over time (Extended Data Fig. 4c). In contrast, colonies cultured in Matrigel had sustained, intermediate levels of nuclear YAP (Extended Data Fig. 4c). We proposed that, although stiff matrices initially enhance YAP activity within ISCs by promoting cellular tension[26,27], the resulting colony growth within a stiff confining environment may give rise to compression, which would lead to YAP inactivation, thus retarding further growth and morphogenesis[26,29].

We therefore sought to design mechanically dynamic matrices, which would afford the higher stiffness initially required for YAP activation and ISC expansion, but would subsequently soften to alleviate the accumulation of compressive forces, and permit *in vitro* organogenesis. Thus, we created hybrid PEG hydrogels wherein a stable polymer

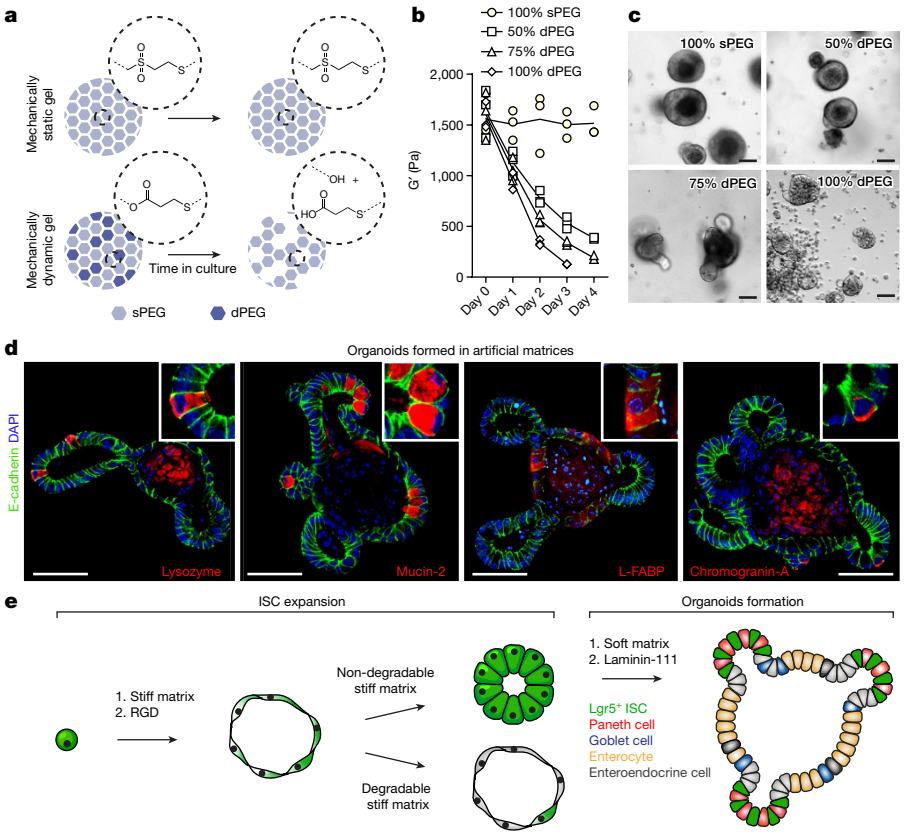

Figure 4 | Intestinal organoid formation within well-defined matrices. **a**, A schematic illustrating the chemical basis of the mechanically dynamic hydrogels. **b**, Mechanical characterization of hybrid sPEG–dPEG gels. For each condition, graph shows individual data points derived from $n = 3$ independently prepared gels and means. G', shear modulus. **c**, Organoid formation within matrices of varying softening rates. **d**, Organoids formed in PEG hydrogels contain differentiated intestinal cells. **e**, Summary of the rules governing different stages of organoid formation within an artificial matrix. Scale bars, 50 μm.

backbone (sPEG, mechanically static PEG) was partially replaced with hydrolytically degradable polymer (dPEG, mechanically dynamic PEG)[30], the presence of which affords sustained gel softening (Fig. 4a). Varying the ratio of sPEG to dPEG within the gels allowed us to control the softening profile over time (Fig. 4b). ISC colony formation in all conditions was extensive. Upon switching the colonies to organoid formation conditions, we found that matrix softening was not sufficient to induce budding in the presence of RGD only (data not shown). In the presence of RGD and laminin-111, but not laminin-derived peptides (Extended Data Fig. 5i), the softening profile of the gels significantly influenced the emergent phenotype (Fig. 4c): organoids formed only in gels with a stiffness of around 190 Pa, suggesting that organoid formation in a minimal environment occurs in a narrow mechanical window. Immunofluorescence analysis demonstrated the presence of differentiated cells within organoids grown in minimal matrices (Fig. 4d). As predicted, at the time of differentiation, the extent of YAP activation was significantly higher in softening matrices, compared with those of constant, high stiffness (Extended Data Fig. 5j). We suggest that this difference accounts for the separate morphogenetic outcomes within the two matrices.

Finally, to test whether these matrices are also suitable for the culture of clinically relevant human counterparts, we embedded human small intestinal and colorectal cancer organoids in PEG RGD matrices. As reported before, growth was less vigorous than that of mouse cells, yet most of the embedded organoids survived and continued to expand (Extended Data Fig. 5k, l), suggesting that the PEG-based hydrogels reported here can be adapted for the culture of human organoids.

We report the first, to our knowledge, synthetic matrix for the expansion of mouse and human ISCs and a minimal matrix for the culture of mouse intestinal organoids. In addition to a final product with a wide range of applications in research and therapy, the design process provides mechanistic insight into how the 3D microenvironment influences multiple aspects of organoid formation, including ISC proliferation, fate decisions and self-organization. YAP has been implicated in the regulation of ISC behaviour, and described as a mechanotransducer in other cellular systems—here we bridge these roles, demonstrating that the YAP-mediated control of ISC self-renewal can have a mechanical upstream component. Notably, elucidating the role of ECM components and physical parameters on ISC behaviour was made possible by the modular nature of the synthetic hydrogels.

In creating a well-defined matrix for intestinal organoids, we identified general design principles that may be adopted in building synthetic scaffolds for different organoid systems. We found that, within a minimal environment, separate stages of the organoid formation process require different microenvironments (Fig. 4e). Indeed, the native cellular environment evolves to accommodate the dynamic needs of tissues during development, homeostasis and repair. Mimicking the dynamic character of native microenvironments in designer matrices may not only replace animal-derived gels for organoid culture, but may also help to enhance the similarity of organoids to real organs.

Online Content Methods, along with any additional Extended Data display items and Source Data, are available in the online version of the paper; references unique to these sections appear only in the online paper.

Received 4 February; accepted 18 October 2016.
Published online 16 November 2016.

1. Clevers, H. Modeling development and disease with organoids. *Cell* **165,** 1586–1597 (2016).
2. Lancaster, M. A. & Knoblich, J. A. Organogenesis in a dish: modeling development and disease using organoid technologies. *Science* **345,** 1247125 (2014).

3. Sasai, Y. Cytosystems dynamics in self-organization of tissue architecture. *Nature* **493,** 318–326 (2013).
4. Fatehullah, A., Tan, S. H. & Barker, N. Organoids as an *in vitro* model of human development and disease. *Nat. Cell Biol.* **18,** 246–254 (2016).
5. Lutolf, M. P., Gilbert, P. M. & Blau, H. M. Designing materials to direct stem-cell fate. *Nature* **462,** 433–441 (2009).
6. Ranga, A. *et al.* 3D niche microarrays for systems-level analyses of cell fate. *Nat. Commun.* **5,** 4324 (2014).
7. Sato, T. & Clevers, H. Growing self-organizing mini-guts from a single intestinal stem cell: mechanism and applications. *Science* **340,** 1190–1194 (2013).
8. Sato, T. *et al.* Single Lgr5 stem cells build crypt-villus structures *in vitro* without a mesenchymal niche. *Nature* **459,** 262–265 (2009).
9. Dekkers, J. F. *et al.* A functional CFTR assay using primary cystic fibrosis intestinal organoids. *Nat. Med.* **19,** 939–945 (2013).
10. Yui, S. *et al.* Functional engraftment of colon epithelium expanded in vitro from a single adult $Lgr5^+$ stem cell. *Nat. Med.* **18,** 618–623 (2012).
11. Kleinman, H. K. & Martin, G. R. Matrigel: basement membrane matrix with biological activity. *Semin. Cancer Biol.* **15,** 378–386 (2005).
12. Jabaji, Z. *et al.* Type I collagen as an extracellular matrix for the *in vitro* growth of human small intestinal epithelium. *PLoS One* **9,** e107814 (2014).
13. Hughes, C. S., Postovit, L. M. & Lajoie, G. A. Matrigel: a complex protein mixture required for optimal growth of cell culture. *Proteomics* **10,** 1886–1890 (2010).
14. Vukicevic, S. *et al.* Identification of multiple active growth factors in basement membrane Matrigel suggests caution in interpretation of cellular activity related to extracellular matrix components. *Exp. Cell Res.* **202,** 1–8 (1992).
15. Seliktar, D. Designing cell-compatible hydrogels for biomedical applications. *Science* **336,** 1124–1128 (2012).
16. Ehrbar, M. *et al.* Biomolecular hydrogels formed and degraded via site-specific enzymatic reactions. *Biomacromolecules* **8,** 3000–3007 (2007).
17. Benoit, Y. D., Groulx, J. F., Gagné, D. & Beaulieu, J. F. RGD-dependent epithelial cell-matrix interactions in the human intestinal crypt. *J. Signal Transduct.* **2012,** 248759 (2012).
18. Simo, P. *et al.* Changes in the expression of laminin during intestinal development. *Development* **112,** 477–487 (1991).
19. Simon-Assmann, P. *et al.* Differential expression of laminin isoforms and α6-β4 integrin subunits in the developing human and mouse intestine. *Dev. Dyn.* **201,** 71–85 (1994).
20. Wang, F. *et al.* Isolation and characterization of intestinal stem cells based on surface marker combinations and colony-formation assay. *Gastroenterology* **145,** 383–395 (2013).
21. Yamamoto, S. *et al.* Heparan sulfate on intestinal epithelial cells plays a critical role in intestinal crypt homeostasis via Wnt/β-catenin signaling. *Am. J. Physiol. Gastrointest. Liver Physiol.* **305,** G241–G249 (2013).
22. Fernández-Sánchez, M. E. *et al.* Mechanical induction of the tumorigenic β-catenin pathway by tumour growth pressure. *Nature* **523,** 92–95 (2015).
23. Guilak, F. *et al.* Control of stem cell fate by physical interactions with the extracellular matrix. *Cell Stem Cell* **5,** 17–26 (2009).
24. Gregorieff, A., Liu, Y., Inanlou, M. R., Khomchuk, Y. & Wrana, J. L. Yap-dependent reprogramming of $Lgr5^+$ stem cells drives intestinal regeneration and cancer. *Nature* **526,** 715–718 (2015).
25. Imajo, M., Ebisuya, M. & Nishida, E. Dual role of YAP and TAZ in renewal of the intestinal epithelium. *Nat. Cell Biol.* **17,** 7–19 (2015).
26. Aragona, M. *et al.* A mechanical checkpoint controls multicellular growth through YAP/TAZ regulation by actin-processing factors. *Cell* **154,** 1047–1059 (2013).
27. Dupont, S. *et al.* Role of YAP/TAZ in mechanotransduction. *Nature* **474,** 179–183 (2011).
28. Sternlicht, M. D. & Werb, Z. How matrix metalloproteinases regulate cell behavior. *Annu. Rev. Cell Dev. Biol.* **17,** 463–516 (2001).
29. Halder, G., Dupont, S. & Piccolo, S. Transduction of mechanical and cytoskeletal cues by YAP and TAZ. *Nat. Rev. Mol. Cell Biol.* **13,** 591–600 (2012).
30. Nicodemus, G. D. & Bryant, S. J. Cell encapsulation in biodegradable hydrogels for tissue engineering applications. *Tissue Eng. Part B Rev.* **14,** 149–165 (2008).

Acknowledgements We thank M. Knobloch (University of Zurich) for helpful discussions, A. Negro (EPFL) for help in the development of PEG–alginate hybrid hydrogels, D. Ossipov (Uppsala University) for providing hyaluronic acid, the Lausanne Genomic Technologies Facility (K. Harshman) for RNA-seq and D. Pioletti (EPFL) for rheometer use. N.G. was supported by an EMBO Long-Term Postdoctoral Fellowship. This work was also supported by funding from the Ecole Polytechnique Fédérale de Lausanne (EPFL). Work performed in the laboratory of H.C. was supported by the NWO Translational Adult Stem Cell Research Grant 40-41400-98-1108 and by a NWO VENI Grant 916.15.182.

Author Contributions N.G. and M.P.L. conceived the study, designed experiments, analysed data and wrote the manuscript. N.G. was involved in performing and analysing all experiments in the manuscript except for those involving human organoids. P.O.M. helped design experiments and analyse RNA-seq data. A.M. performed qPCR gene expression experiments and analysed data and produced lentiviruses. S.G. performed flow cytometry analysis of integrin expression of ISCs culture in Matrigel and PEG RGD. M.E.B. designed and characterized PEG–alg hydrogel system and helped N.G. perform experiments with ISCs in these matrices. N.S. and H.C. designed experiments and analysed data with human cells. N.S. performed experiments with human cells.

Author Information Reprints and permissions information is available at www.nature.com/reprints. The authors declare competing financial interests: details are available in the online version of the paper. Readers are welcome to comment on the online version of the paper. Correspondence and requests for materials should be addressed to M. L. (matthias.lutolf@epfl.ch).

Reviewer Information *Nature* thanks L. Li, J. Mills and the other anonymous reviewer(s) for their contribution to the peer review of this work.

METHODS

Data reporting. The experiments were not randomized and the investigators were not blinded to allocation during experiments and outcome assessment. No statistical methods were used to determine sample size.

Mice. Intestinal crypts were extracted from 5–10-week-old heterozygous Lgr5–eGFP-IRES-CreERT2 mice (Jackson Laboratory), following animal experimentation protocols prescribed by EPFL and FELASA.

Intestinal crypt isolation. Murine intestinal crypts were isolated following procedures described previously. In brief, the proximal part of the intestine was collected, opened longitudinally and washed with ice-cold PBS. The luminal side of the intestine was scraped using a glass slide to remove luminal content and villous structures. After washing with ice-cold PBS again, the intestine was cut into 2–4 mm pieces with scissors. The pieces were transferred to a 50 ml Falcon tube and further washed with cold PBS (5–10 times) with gentle vortexing. Intestinal fragments were then incubated in 20 mM EDTA/PBS for 20 min on ice. EDTA was removed, 10 ml of cold PBS was added and crypts were released by manual shaking of the suspension for 5 min. The supernatant was collected and passed through a 70-μm strainer (BD Biosciences). The remaining tissue fragments were resuspended in 10 ml cold PBS, triturated 5–10 times and the supernatant was passed through a 70-μm strainer. The previous step was repeated a second time. The three crypt-containing fractions were combined and centrifuged at 110*g* for 5 min. The pellet was resuspended in 10 ml cold Advanced DMEM/F12 (Invitrogen) and centrifuged at 84*g* to remove single cells and tissue debris. The resulting pellet was enriched in crypts, which were subsequently dissociated or directly embedded in PEG gels or in Matrigel (BD Biosciences; growth factor reduced, phenol red-free formulation). When needed, crypts or ISC colonies were dissociated enzymatically by incubating for 8 min at 37 °C in 1 ml TrypLE Express (Life Technologies), supplemented with DNase I (2000 U ml^{-1}; Roche), 0.5 mM *N*-acetylcysteine (Sigma) and 10 μM Y27632 (Stemgent). Undigested clusters were removed by passing the suspension through a 40 μm strainer.

Cell culture. Freshly isolated mouse crypts or single cells from dissociated mouse ISC colonies were embedded in Matrigel or PEG gels, which were cast into 20-μl droplets at the bottom of wells in 24-well plate. Following polymerization (15 min, 37 °C), the gels were overlaid with 500 μl of ISC expansion medium (Advanced DMEM/F12 containing Glutamax, HEPES, penicillin-streptomycin, B27, N2 (Invitrogen) and 1 μM *N*-acetylcysteine (Sigma)), supplemented with growth factors, including EGF (50 ng ml^{-1}; R&D), Noggin (100 ng ml^{-1}; produced in-house) and R-spondin (500 ng ml^{-1}; produced in-house), and small molecules, including CHIR99021 (3 μM; Millipore) and valproic acid (1 mM; Sigma). For single-cell culture, thiazovivin (2.5 μM; Stemgent) was included in the medium during the first two days. To induce stem cell differentiation and organoid formation, the medium was removed, the gels were washed with PBS and fresh medium containing EGF, Noggin and R-spondin was added. Human small intestinal and colorectal cancer organoids were generated as described previously[31,32] and grown in 20-μl droplets of Matrigel or PEG gels overlaid with Advanced DMEM/F12 containing Glutamax, HEPES, penicillin-streptomycin, B27 (Life Technologies), Wnt3a (50% conditioned medium; produced in-house; only for small intestinal organoids), R-spondin 1 (20% conditioned medium; produced in-house), Noggin (10% conditioned medium; produced in-house), *N*-acetylcysteine (2 μM; Sigma), Nicotinamide (10 mM; Sigma), human EGF (50 ng ml^{-1}; Peprotech), A83-01 (500 nM; Tocris), SB202190 (10 μM; Sigma), Prostaglandin E2 (10 nM; Tocris); Gastrin (10 nM; Tocris), and Y-27632 (10 μM; Abmole). In general, growth factors were replenished every two days, with full medium change taking place every four days. Where indicated, the following compounds were used at the specified concentrations: blebbistatin (Sigma, 12.5 μM), ML7 (Calbiochem, 10 μM), cytochalasin D (Merck-Millipore, 0.1 μg ml^{-1}), echistatin (Sigma, 500 nM).

PEG, peptides and synthesis of hydrogel precursors. Vinylsulfone-functionalized 8-arm PEG (8-arm PEG-VS or sPEG) was purchased from NOF, and acrylate-functionalized 8-arm PEG (8-arm PEG-Acr or dPEG) was purchased from Creative PEGWorks. The transglutaminase (TG) factor XIII (FXIIIa) substrate peptides Ac-FKGGGPQGIWGQ-ERCG-NH2 (TG-DG-Lys), Ac-FKGG-GDQGIAGF-ERCG-NH2 (TG-NDG-Lys) and H-NQEQVSPL-ERCGNH2 (TG-Gln) and the RGD-presenting adhesion peptide H-NQEQVSPL-RGDSPG-NH2 (TG-Gln-RGD) were purchased from GL Biochem. To couple the FXIIIa substrate peptides to the 8-arm PEG-VS or 8-arm PEG-Acr, they were mixed with the PEG powder in a 1.2 stoichiometric excess (peptide-to-VS group); the combined solids were dissolved in triethanolamine (0.3 M, pH 8.0), and allowed to react for 2 h at 37 °C. The reaction solution was dialysed (Snake Skin, MWCO 10K, PIERCE) against ultrapure water for 3 days at 4 °C, after which the five products ((PEG-VS)-DG-Lys, (PEG-VS)-NDG-Lys, (PEG-VS)-Gln, (PEG-Acr)-NDG-Lys, (PEG-Acr)-Gln) were lyophilized. The resulting solid precursors were dissolved in ultra-pure water to make 13.33% w/v stock solutions.

Formation and dissociation of PEG hydrogels. Appropriate volumes of 13.33% w/v PEG precursor solutions were mixed in stoichiometrically balanced ratios to generate hydrogel networks of a desired final PEG content. Hydrogel formation was triggered by the addition of thrombin-activated FXIIIa (10 U ml^{-1}; Galexis) in the presence of Tris-buffered saline (TBS; 50 mM, pH 7.6) and 50 mM $CaCl_2$. The spare reaction volume was used for the incorporation of dissociated ISCs, fragments of human small intestinal or colorectal cancer organoids, and ECM components: TG-RGD-Gln, fibronectin (0.5 mg ml^{-1}; Invitrogen), laminin-111 (0.1 mg ml^{-1}; Invitrogen), collagen-IV (0.25 mg ml^{-1}; BD Bioscience), hyaluronic acid (0.5 mg ml^{-1}; gift from D. Ossipov, Uppsala University), perlecan (0.05 mg ml^{-1}; Sigma). Gels were allowed to crosslink by incubating at 37 °C for 15 min. Dissociation and release of colonies grown in PEG for downstream cell processing or re-embedding was accomplished by enzymatic digestion of the gels. Gels were carefully detached from the bottom of the plate using the tip of a metal spatula and transferred to a 15-ml Falcon tube containing 1 ml of TrypLE Express (Life Technologies), supplemented with DNase I (2,000 U ml^{-1}; Roche), 0.5 mM N-acetylcysteine (Sigma) and 10 μM Y27632 (Stemgent). Following digestion (10 min, 37 °C), the cell suspension was washed with 10 ml of cold medium, passed through a 40-μm strainer (BD Biosciences) and centrifuged at 1,200 r.p.m. for 5 min.

Softening of PEG hydrogels through ester-based hydrolysis. To form mechanically dynamic PEG hydrogels, which underwent varying extents of spontaneous softening, hybrid hydrogels were formed from both PEG-VS and PEG-Acr hydrogel precursors. Specifically, to form a fast-softening 100% Acr gel, stoichiometric quantities of (PEG-Acr)-NDG-Lys and (PEG-Acr)-Gln precursors were allowed to crosslink. A slow-softening 50% Acr gel was formed by crosslinking stoichiometric amounts of (PEG-VS)-NDG-Lys and (PEG-Acr)-Gln precursors. A 75% Acr gel with intermediate kinetics of softening was formed by crosslinking the (PEG-Acr)-Gln precursor with half of the stoichiometric equivalent of (PEG-VS)-NDG-Lys and half of the stoichiometric equivalent of (PEG-Acr)-NDG-Lys. Regardless of the relative proportions of (PEG-VS) and (PEG-Acr) precursors within the hydrogel, its overall PEG content was varied to tune its initial mechanical properties. It should be noted that, by providing an initially stiff and later a soft environment, the mechanically dynamic matrices support both ISC expansion and organoid formation. Hence, ISCs can be expanded and organoids can be formed in the same hydrogel.

PEG–alginate hydrogels for controlled matrix softening. Hybrid PEG–alginate (PEG–alg) gels were employed to induce a controlled drop in stiffness at a desired time. PEG–alg gels were formed by the simultaneous presence of activated FXIII enzyme—to drive the crosslinking of the PEG macromers—and Ca^{2+} ions, which induce the crosslinking of the alginate polysaccharides. Hybrid gels were formed by casting a solution, containing 2% (w/v) of stoichiometrically balanced (PEG-VS)-NDG-Lys and (PEG-VS)-Gln precursors, 10 mM TG-RGD-Gln, 10 U ml^{-1} FXIIIa, 0.8% (w/v) alginate (Sigma) and dissociated ISCs, within a 1% agarose/2% gelatin mould, containing 20 mM $CaCl_2$. The solution was incubated at 37 °C for 15 min, carefully de-molded from the agarose substratum and transferred to a 12-well plate containing 1 ml of complete ISC expansion medium. Matrix softening was induced at the desired time by adding 1 U ml^{-1} alginate lyase (Sigma), and incubating for 1 h at 37 °C. The digested gels were washed and transferred to freshly prepared ISC expansion medium.

Mechanical characterization of PEG hydrogels. The shear modulus of the PEG gels was determined by performing small-strain oscillatory shear measurements on a Bohlin CVO 120 rheometer. In brief, preformed hydrogel discs 1–1.4 mm in thickness were allowed to swell in complete cell culture medium for at least 3 h, and were subsequently sandwiched between the parallel plates of the rheometer. The mechanical response of the gels was recorded by performing frequency sweep (0.1–10 Hz) measurements in a constant strain (0.05) mode, at 37 °C. The shear modulus (G') is reported as a measure of gel mechanical properties.

Quantification of ISC colony formation efficiency, ISC colony shape, morphology and Lgr5 expression. To quantify the colony formation efficiency of single embedded ISCs, phase contrast *z*-stacks spanning the entire thickness of the cell-laden Matrigel or PEG gels were collected (Zeiss Axio Observer Z1) at 5 different locations within the gels. The Cell Counter plugin in ImageJ (NIH) was used to quantify the fraction of cells which had formed colonies at day 4 after seeding. To quantify colony circularity, phase contrast images of ISC colonies grown in the condition of interest (between 5 and 38 colonies per condition) were taken, and their contours traced manually in ImageJ. The circularity of the contours was measured using the Measure algorithm in ImageJ. To characterize the cell morphology within ISC colonies grown in different conditions, phase contrast images of at least 50 colonies were taken and the numbers of colonies containing packed columnar cells versus spread cells were counted. To quantify Lgr5 expression within ISC colonies grown within different matrices, fluorescence images of at least 50 colonies

per condition were recorded and the number of colonies expressing Lgr5–eGFP was counted.

Laminin peptide hydrogels. To identify a short sequence that supports intestinal organoid culture, we created a library of soft (G′ = 200 Pa) hydrogels in which binding sequences from the laminin α1 subunit previously shown to be biofunctional[33,34] (Extended Data Table 4) were tethered to the PEG backbone. Embedding fragments of pre-formed organoids and screening the library for organoid survival and growth revealed that two laminin-derived peptides—AG73 and A55—significantly enhanced organoid viability and supported further growth (Extended Data Fig. 5a). Presenting these two sequences (A55 and AG73) alongside in the same gel did not appear to have an additive effect, likely owing to a redundant adhesion mechanism. Hence, we focused on the sequence with a stronger individual effect, that is, AG73 and the corresponding PEG gels (referred to as TG PEG-AG73). Varying the amount of AG73 peptide tethered to the PEG gel backbone revealed a dose-dependent effect on intestinal organoid viability and growth (Extended Data Fig. 5b, c). Despite the improved rate of survival and morphogenesis in TG PEG-AG73 matrices compared with plain PEG or PEG RGD, the process was significantly less efficient compared with Matrigel, and morphological differences were apparent. Keeping in mind that the effect of AG73 was concentration-dependent, we attributed these differences to a potentially sub-optimal AG73 ligand density within the synthetic system. By design, there is an upper limit to the concentration of tethered factors that can be incorporated into the PEG system used thus far in the study: exceeding this limit disrupts the structural integrity of the gels. To overcome this limitation and enhance the biofunctionality of the synthetic matrix by increasing the concentration of AG73 ligands, we turned to chemically crosslinked PEG gels. Here, vinyl sulfone (VS)-conjugated 4-arm PEG precursors are covalently linked into solid hydrogels through Michael-type addition between VS groups and the thiols of a short crosslinker containing two cysteine residues. To incorporate the AG73 ligand at a high density, we designed a crosslinker in which the AG73 sequence was flanked by two short cysteine-containing sequences. The resulting gels (hereafter referred to as MT PEG-AG73) presented the AG73 ligand at a concentration of 3.1 mM, thus significantly surpassing the highest concentration achieved in the enzymatically crosslinked matrices. Embedding intestinal organoid fragments into MT PEG-AG73 revealed that the percentage of tissues that remained viable and continued to undergo morphogenesis approached that observed in Matrigel (Extended Data Fig. 5e). To verify the maintenance of ISCs within the organoids grown in MT PEG-AG73, we embedded tissues extracted from the Lgr5-eGFP reporter mouse and monitored eGFP expression. We observed that Lgr5–eGFP was expressed in the expected pattern: localized to the crypt-like buds of the organoids (Extended Data Fig. 5f). The fraction of organoids expressing the marker was significantly higher than in those cultured in TG PEG AG73, and at least as high as in organoids cultured in Matrigel (Extended Data Fig. 5g). We also confirmed that the organoids cultured in MT PEG-AG73 were polarized and contained differentiated cells (Extended Data Fig. 5h).

Immunofluorescence analysis. ISC colonies or organoids embedded in Matrigel or PEG gels were fixed with 4% paraformaldehyde (PFA) in PBS (30 min, room temperature). The fixation process typically led to complete degradation of the Matrigel. Suspended tissues were collected and centrifuged (800 r.p.m., 5 min) to remove the PFA, washed with ultra-pure water and pelleted. Following resuspension in water, the organoids were spread on glass slides and allowed to attach by drying. Attached organoids were rehydrated with PBS. Following fixation, organoids embedded in PEG or spread on glass were permeabilized with 0.2% Triton X-100 in PBS (1 h, room temperature) and blocked (10% goat serum in PBS containing 0.01% Triton X-100) for at least 3 h. Samples were subsequently incubated overnight at 4 °C with phalloidin-Alexa 546 (Invitrogen) and primary antibodies against lysozyme (1:50; Thermo Scientific PA1-29680), mucin-2 (1:50; Santa Cruz sc-15334), chromogranin-A (1:50; Santa Cruz sc-13090), L-FABP (1:50; Santa Cruz sc-50380) and YAP1 (1:50; Santa Cruz sc-101199) diluted in blocking buffer. After washing with PBS for at least 3 h, samples were incubated overnight at 4 °C with secondary antibody Alexa 647 goat-α-rabbit (1:1000 in blocking solution; Invitrogen). Following extensive washing, stained organoids were imaged in epifluorescence (Zeiss Axio Observer Z1) or confocal (Zeiss LSM 710) mode. Alternatively, ISC colonies or organoids cultured in PEG were released from the hydrogel before PFA fixation, by incubating the gels with 1 mg ml^{-1} Dispase (Gibco) for 7 min at 37 °C. The released colonies or organoids were fixed with PFA in suspension, and attached to glass coverslips, as described above.

Immunohistochemical analysis of human organoids. Human organoids were fixed in 10% neutral buffered formalin, washed with PBS, dehydrated, and embedded in paraffin. Sections were stained with H&E or Ki67 antibody (1:250; Monosan).

Lentivirus production and transduction. Lentiviral particles encoding for shRNA recognizing YAP (two sequences validated for knockdown, purchased from Sigma) or the pLKO.1-puro Non-Target control shRNA (Sigma) were generated in HEK 293T cells, using third generation lentivirus packaging vectors. Transfection was carried out using the X-tremeGENE HP Transfection kit (Roche). After 48 h, the supernatant was collected, filtered and ultracentrifuged at 50,000*g* for 2 h at 20 °C. The resulting pellet was resuspended in PBS and stored at −80 °C. Lentiviral infection of ISCs was performed by dissociating the ISC colonies (described above), resuspending the resulting single cells in ice-cold liquid Matrigel, containing 10 μM Y27632 and the concentrated lentiviral particles at a dilution of 1:10. ISCs were incubated with viral particles in a liquid suspension for 45 min on ice. The suspension was subsequently cast into droplets and allowed to form gels, which were overlaid with ISC expansion medium. The embedded ISCs proceeded to form colonies, which carried the transgene encoded by the virus. The cells were allowed to recover and form colonies for 36 h, after which they were dissociated and encapsulated within PEG hydrogels or used for quantification of knockdown efficiency by qPCR.

Quantitative real-time PCR (qPCR). ISC colonies or organoids grown in Matrigel or PEG gels were dissociated as described above, and RNA was extracted using an RNeasy Micro Kit (Qiagen). cDNA was synthesized using the iScript cDNA Synthesis Kit (Bio-Rad). qPCR was carried out using the Power SYBR Green PCR Master Mix (Applied Biosystems) and the primers listed Extended Data Table 1.

RNA-seq: library preparation, sequencing, data processing, statistical analysis, interpretation and accession numbers. RNA-seq libraries were prepared using 500 ng of total RNA and the Illumina TruSeq Stranded mRNA reagents (Illumina; San Diego, California, USA) on a Sciclone liquid handling robot (PerkinElmer; Waltham, Massachusetts, USA) using a PerkinElmer-developed automated script. Cluster generation was performed with the resulting libraries using the Illumina TruSeq SR Cluster Kit v4 reagents and sequenced on the Illumina HiSeq 2500 using TruSeq SBS Kit v4 reagents. Sequencing data were processed using the Illumina Pipeline Software version 1.84. Purity-filtered reads were adapters and quality trimmed with Cutadapt and filtered for low complexity with seq_crumbs (v. 0.1.8). Reads were aligned against the *Mus musculus*.GRCm38.82 genome using STAR[35]. The number of read counts per gene locus was summarized with htseq-count[36] using the *Mus musculus*.GRCm38.82 gene annotation. Quality of the RNA-seq data alignment was assessed using RSeQC[37]. Reads were also aligned to the *Mus musculus*.GRCm38.82 transcriptome using STAR and the estimation of the isoforms abundance was computed using RSEM[38]. Statistical analysis was performed for genes in the R software package. Genes with low counts were filtered out according to the rule of 1 count per million in at least 1 sample. Library sizes were scaled using TMM normalization in the EdgeR package[39] and log-transformed with the limma voom function[40]. Differential expression was computed with limma[41] by fitting paired samples data into a linear model and performing all pairwise comparisons. To control for false discovery and multiple testing, we computed an adjusted *P* value, using the Benjamini–Hochberg method. Gene set expression analysis was performed with the freely available GSEA software[42] (Broad Institute), using differential expression values and pre-defined gene signatures as inputs. In particular, to test for upregulation of stress-related genes, the MSigDB gene set 'BIOCARTA_STRESS_PATHWAY' was used. We checked for upregulation of colon cancer-related genes by using the inflammatory colon cancer signature, as identified by Sadanandam *et al.*[43]. Functional annotation and gene ontology analysis of significantly enriched gene sets was conducted using the MetaCore software. The accession numbers for the gene expression profiles described here are GEO: GSE85391.

Statistical analysis and sample information. Statistically significant differences between the means of two groups were assessed by using a Student's *t*-test, whereas data containing more than two experimental groups were analysed with a one-way ANOVA followed by a Bonferroni's multiple comparison test. All statistical analyses were performed in the GraphPad Prism 6.0 software.

Data availability. RNA sequencing data that support the findings of this paper have been deposited to the Gene Expression Omnibus (GEO) public repository (GSE85391; https://www.ncbi.nlm.nih.gov/geo/query/acc.cgi? acc=GSE85391). Source Data for Figs. 1–4 and Extended Data Figs 1–5 are provided with the paper. All additional relevant data are available upon request from the corresponding author.

31. Matano, M. *et al.* Modeling colorectal cancer using CRISPR–Cas9-mediated engineering of human intestinal organoids. *Nat. Med.* **21,** 256–262 (2015).
32. Sato, T. *et al.* Long-term expansion of epithelial organoids from human colon, adenoma, adenocarcinoma, and Barrett's epithelium. *Gastroenterology* **141,** 1762–1772 (2011).

33. Dobin, A. *et al.* STAR: ultrafast universal RNA-seq aligner. *Bioinformatics* **29,** 15–21 (2013).
34. Anders, S., Pyl, P. T. & Huber, W. HTSeq—a Python framework to work with high-throughput sequencing data. *Bioinformatics* **31,** 166–169 (2015).
35. Wang, L., Wang, S. & Li, W. RSeQC: quality control of RNA-seq experiments. *Bioinformatics* **28,** 2184–2185 (2012).
36. Li, B. & Dewey, C. N. RSEM: accurate transcript quantification from RNA-Seq data with or without a reference genome. *BMC Bioinformatics* **12,** 323 (2011).
37. Robinson, M. D., McCarthy, D. J. & Smyth, G. K. edgeR: a Bioconductor package for differential expression analysis of digital gene expression data. *Bioinformatics* **26,** 139–140 (2010).
38. Law, C. W., Chen, Y., Shi, W. & Smyth, G. K. voom: Precision weights unlock linear model analysis tools for RNA-seq read counts. *Genome Biol.* **15,** R29 (2014).
39. Ritchie, M. E. *et al.* limma powers differential expression analyses for RNA-sequencing and microarray studies. *Nucleic Acids Res.* **43,** e47 (2015).
40. Subramanian, A. *et al.* Gene set enrichment analysis: A knowledge-based approach for interpreting genome-wide expression profiles. *Proc. Natl Acad. Sci. USA* **102,** 15545–15550 (2005).
41. Sadanandam, A. *et al.* A colorectal cancer classification system that associates cellular phenotype and responses to therapy. *Nat. Med.* **19,** 619–625 (2013).
42. Nomizu, M. *et al.* Identification of cell binding sites in the laminin $\alpha 1$ chain carboxyl-terminal globular domain by systematic screening of synthetic peptides. *J. Biol. Chem.* **270,** 20583–20590 (1995).
43. Nomizu, M. *et al.* Cell binding sequences in mouse laminin $\alpha 1$ chain. *J. Biol. Chem.* **273,** 32491–32499 (1998).

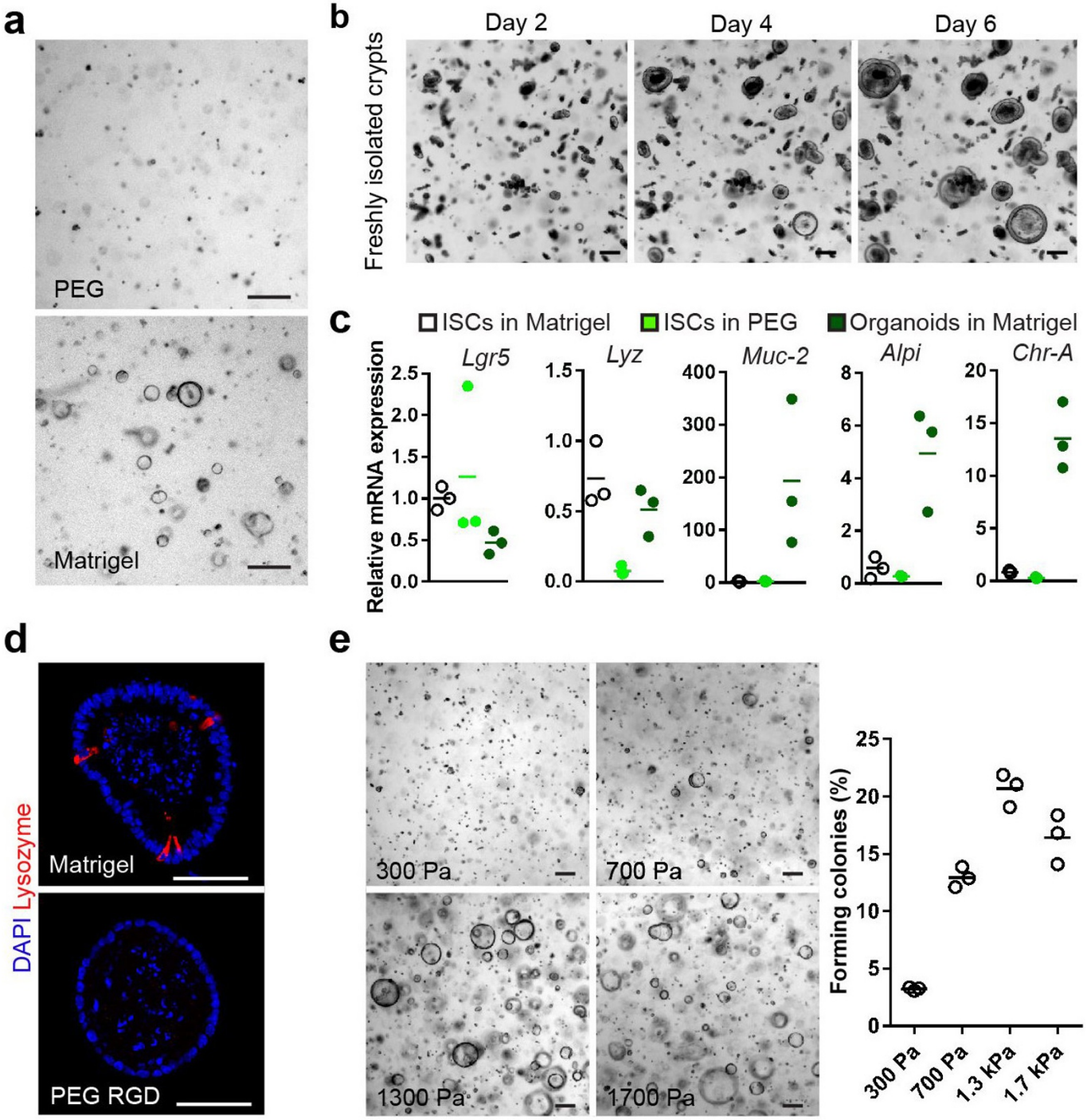

Extended Data Figure 1 | Primary crypt culture in synthetic matrices, characterization of ISCs grown in PEG RGD culture with or without CHIR99021 and valproic acid. a, ISCs cultured in Matrigel and unmodified PEG gels for 24 h. **b**, ISC colonies formed from freshly isolated mouse intestinal crypts embedded in PEG RGD. **c**, Relative mRNA levels of intestinal genes, quantified by qPCR. **d**, ISC colonies cultured under self-renewal conditions in Matrigel, but not PEG gels, contain lysozyme-expressing Paneth cells. **e**, Stiffness-dependent colony formation and quantification of ISCs cultured with EGF, noggin, R-spondin and Wnt3a. Graphs show individual data points derived from $n = 3$ independent experiments and means. Scale bars, 50 μm.

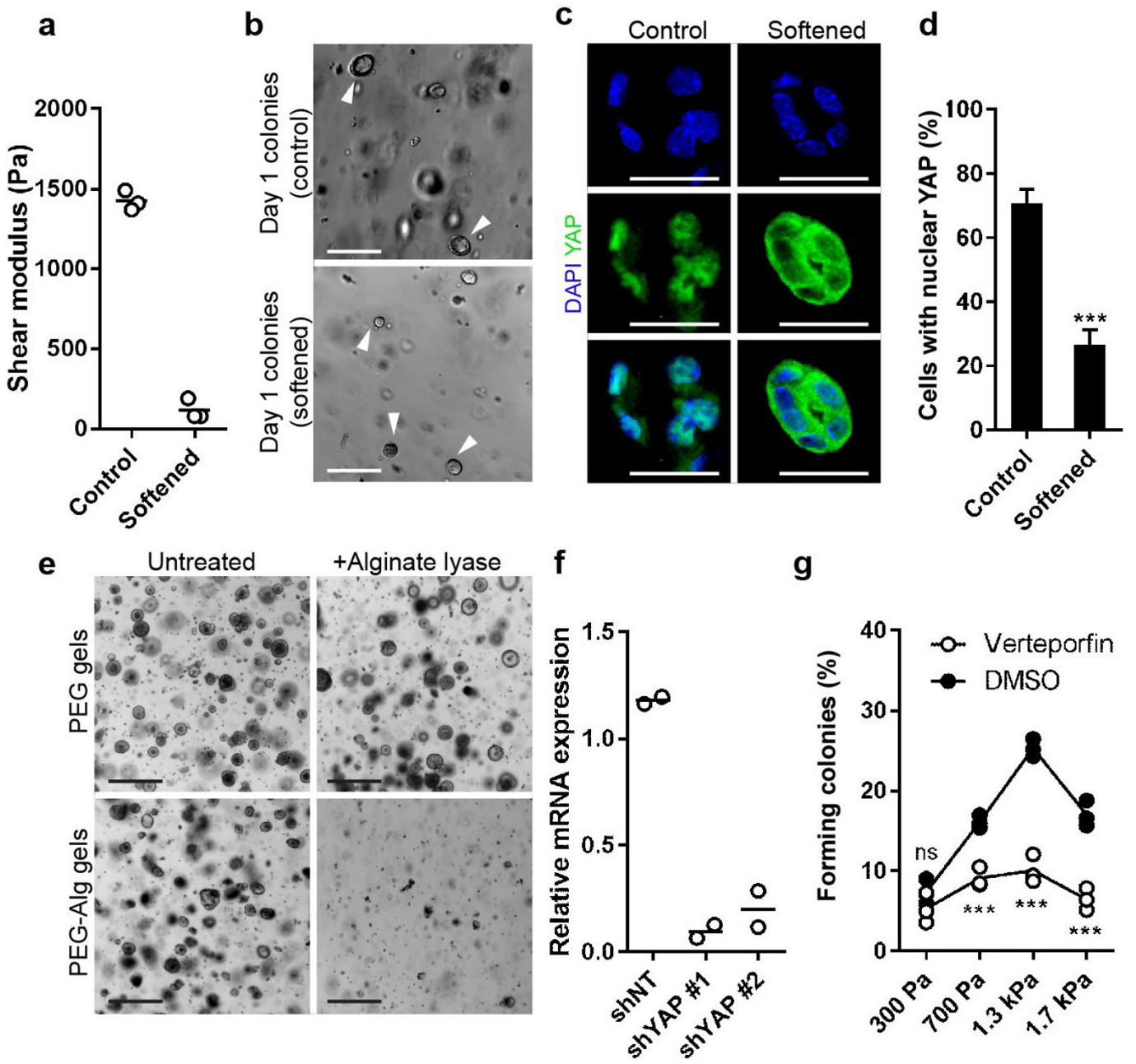

Extended Data Figure 2 | Effect of controlled matrix softening on ISC colony morphology, YAP activity and growth. a, Mechanical properties of control and softened PEG alginate (PEG–alg) hybrid gels obtained by selective degradation of the alginate network. Graph shows individual data points derived from 3 independently prepared gels. **b**, Morphology of day 1 colonies in control and softened PEG–alg gels. **c**, **d**, Distribution of YAP in day 1 colonies in control and softened PEG–alg gels (**c**) and quantification (**d**). $n = 28$ colonies (control) and $n = 31$ (softened). Data are represented as mean ± s.e.m. **e**, Alginate lyase treatment does not affect colony growth in PEG RGD gels. Softening of PEG–alg gels by alginate-lyase-mediated digestion blocks colony growth. **f**, Quantification of shRNA-mediated knockdown of YAP. Graph shows individual data points derived from 2 independent experiments and means. **g**, Effect of verteporfin on ISC colony formation in PEG RGD. Graph shows individual data points derived from 3 independent experiments and means.*$P < 0.05$; **$P < 0.01$; ***$P < 0.01$. Scale bars, 50 μm.

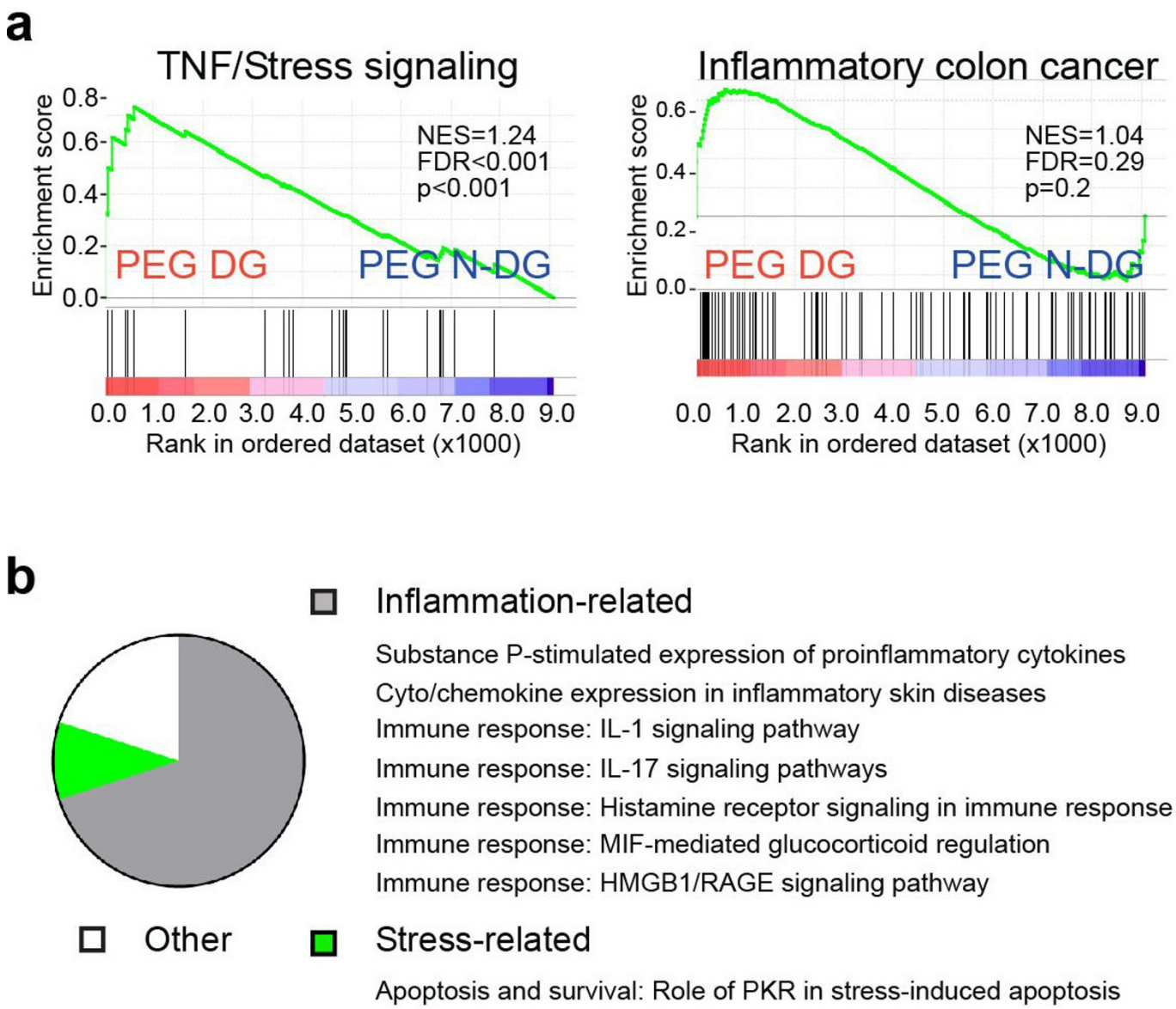

Extended Data Figure 3 | Stiff degradable matrices induce an inflammation-like state in ISCs. a, Gene set enrichment analysis (GSEA) comparing RNA-seq gene expression data of ISCs cultured in degradable compared to non-degradable matrices to published gene signatures (see Methods for details). **b**, Functional annotation of signalling pathway significantly upregulated in degradable matrices (details and statistics shown in Extended Data Tables 2, 3).

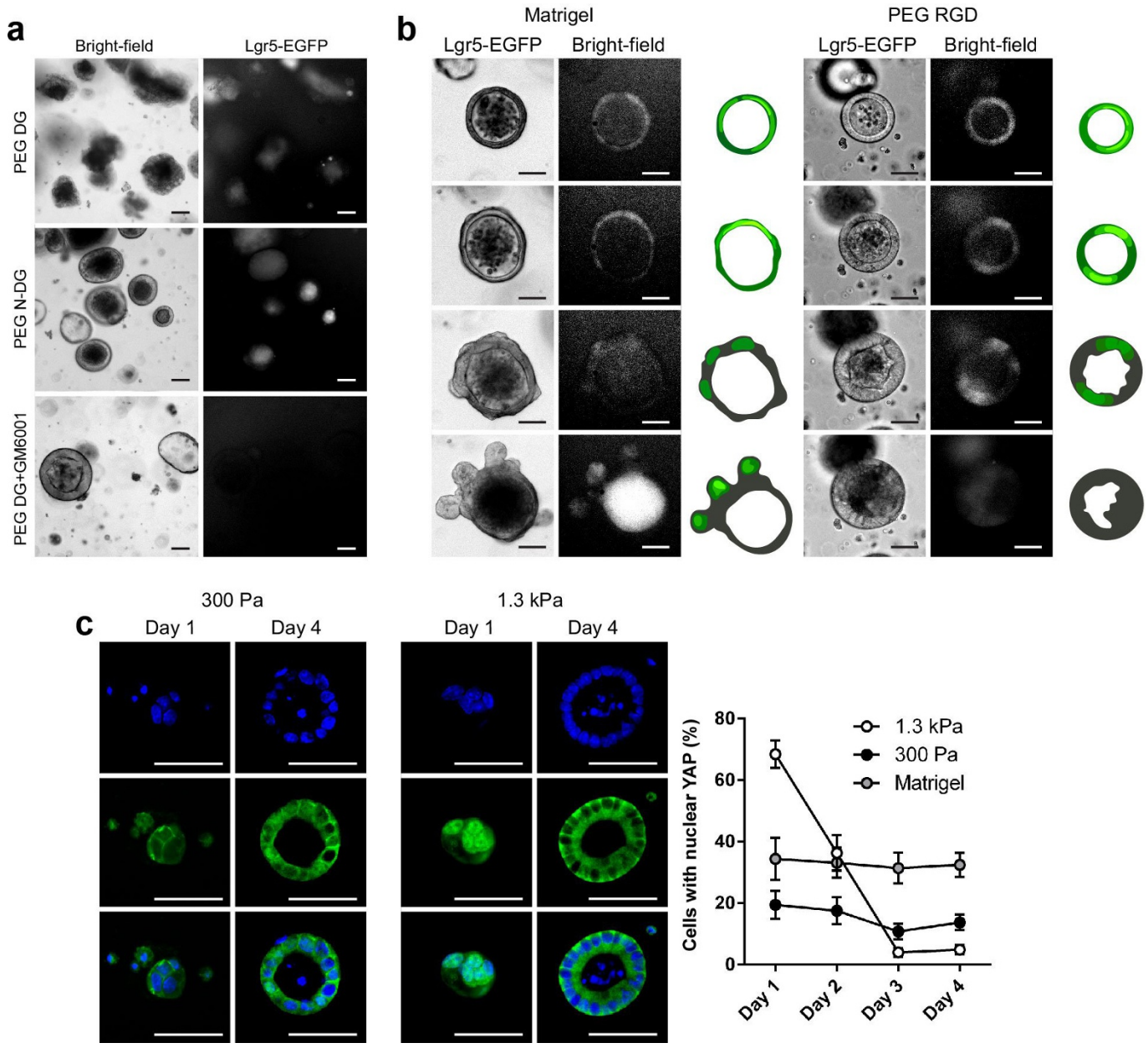

Extended Data Figure 4 | Comparison of organoid formation and YAP activity in Matrigel and PEG RGD. a, Organoid formation does not occur within synthetic PEG RGD matrices. ISC colonies cultured in non-degradable (PEG N-DG) and degradable (PEG DG) PEG RGD matrices, with or without GM6001 for 4 d, and subsequently cultured under organoid formation conditions for 2 d. **b**, Time-course analysis of morphology and Lgr5–eGFP expression during organoid formation. ISC colonies formed in Matrigel and PEG hydrogels were monitored for 48 h, following a switch to differentiation and organoid formation conditions. **c**, Localization of YAP at day 1 and day 4 in ISC colonies formed in 300 Pa and 1.3 kPa PEG RGD gels. **d**, Quantification of nuclear translocation of YAP as a function of time in 300 Pa, 1.3 kPa PEG RGD and Matrigel. Data are shown as means ± s.e.m. To assess the extent of YAP nuclear translocation, $n = 21$ (day 1, 1.3 kPa); 27 (day 2, 1.3 kPa); 22 (day 3, 1.3 kPa); 22 (day 4, 1.3 kPa); 27 (day 1, 300 Pa); 6 (day 2, 300 Pa); 23 (day 3, 300 Pa); 22 (day 4, 300 Pa); 30 (day 1, Matrigel); 28 (day 2, Matrigel); 30 (day 3, Matrigel); 30 (day 4, Matrigel). $^{*}P < 0.05$; $^{**}P < 0.01$; $^{***}P < 0.001$. Scale bars, 50 μm.

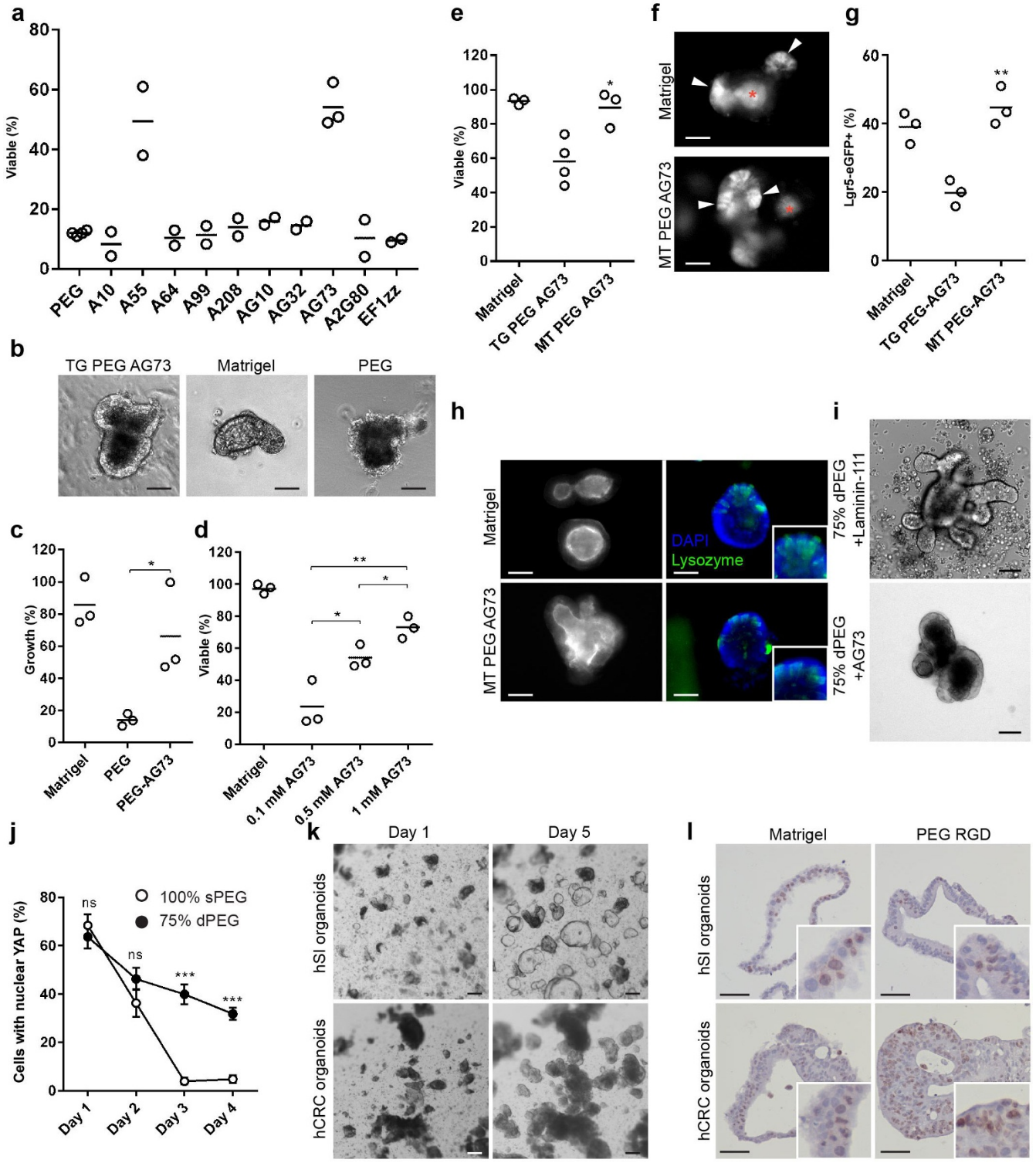

Extended Data Figure 5 | Effect of laminin-derived peptides on organoid formation, and human organoid expansion in PEG RGD. **a**, Effect of different laminin-111-derived sequences on intestinal organoid viability. **b**, Morphology of intestinal organoids grown in Matrigel, plain PEG or PEG-AG73 gels. **c**, AG73-conjugated PEG matrices significantly enhance the growth of intestinal organoids. **d**, Effect of AG73 on intestinal organoid viability and growth is concentration-dependent. **e**, Quantification of intestinal organoid viability in Matrigel, TG PEG-AG73 and MT PEG-AG73. **f**, Morphology and Lgr5–eGFP expression in intestinal organoids grown in Matrigel and MT PEG-AG73 gels. **g**, Quantification of Lgr5–eGFP expression in intestinal organoids expanded in Matrigel, TG PEG-AG73 and MT PEG-AG73. **h**, Establishment of apicobasal polarity and presence of Paneth (lysozyme) cells within organoids grown in MT PEG-AG73. **i**, AG73 peptides are not capable of supporting differentiation and organoid formation from ISC colonies, whereas full-length laminin-111 is. **j**, Quantification of nuclear translocation of YAP as a function of time in cells cultiured within mechanically stable and softening gels. Data are shown as means ± s.e.m. To assess the extent of YAP nuclear translocation, $n = 21$ (day 1, 100% sPEG), 27 (day 2, 100% sPEG), 22 (day 3, 100% sPEG), 22 (day 4, 100% sPEG), 30 (day 1, 75% dPEG), 30 (day 2, 75% dPEG), 30 (day 3, 75% dPEG), and 30 (day 4, 75% dPEG) colonies were analysed. **k**, **l**, Phase contrast images (**k**) and Ki67 expression (**l**) of human ISC colonies and human patient-derived colorectal cancer organoids grown in PEG RGD. Graphs show individual data points derived from $n = 2$ (**a**), $n = 3$ (**c**–**e**, **g**) independent experiments and means. $^{*}P < 0.05$; $^{**}P < 0.01$; $^{***}P < 0.001$. Scale bars, 50 μm.

Extended Data Table 1 | Primers used for qPCR analysis of intestinal gene expression

Mouse gene	Forward primer	Reverse primer
Lgr5	ATTCGGTGCATTTAGCTTGG	CGAACACCTGCGTGAATATG
Alpi	GCCTATCTCTGTGGGGTCAA	TTTCTTGGCACGGTACATCA
ChgA	AAGGTGATGAAGTGCGTCCT	GGTGTCGCAGGATAGAGAGG
Muc2	CCGACTTCAACCCAAGTGAT	GAGCAAGGGACTCTGGTCTG
Lyz1	GTCACACTTCCTCGCTTTCC	TGGCTTTGCTGACTGACAAG
Gapdh	ATCCTGCACCACCAACTGCT	GGGCCATCCACAGTCTTCTG
Yap1	TCCTCCTTTGAGATCCCTGA	GCCATGTTGTTGTCTGATCG

Extended Data Table 2 | Functional annotation of genes significantly upregulated in degradable PEG RGD matrices versus non-degradable PEG RGD matrices, in terms of cellular pathways

Pathway	Count	%	p value	FDR
Immune response_MIF-mediated glucocorticoid regulation	4	17.4	1.7E-05	4.1E-03
Protein folding and maturation_Posttranslational processing of neuroendocrine peptides	5	17.4	2.3E-05	4.1E-03
Immune response_Substance P-stimulated expression of proinflammatory cytokines via MAPKs	4	10.0	2.1E-04	1.9E-02
Immune response_IL-1 signaling pathway	4	9.3	2.3E-04	1.9E-02
Immune response_Histamine H1 receptor signaling in immune response	4	9.1	3.2E-04	1.9E-02
Muscle contraction_Relaxin signaling pathway	4	8.3	3.2E-04	1.9E-02
PDE4 regulation of cyto/chemokine expression in inflammatory skin diseases	4	8.3	3.8E-04	1.9E-02
Apoptosis and survival_Role of PKR in stress-induced apoptosis	4	8.0	4.8E-04	1.9E-02
Immune response_HMGB1/RAGE signaling pathway	4	7.5	4.8E-04	1.9E-02
Immune response_IL-17 signaling pathways	4	7.5	7.7E-04	2.7E-02

Performed using the Metacore software package.

Extended Data Table 3 | Functional annotation of genes significantly upregulated in degradable PEG RGD matrices versus non-degradable PEG RGD matrices, in terms of cellular processes

Process	Count	%	p value	FDR
Chemotaxis	7	5.1	6.1E-05	6.2E-03
Inflammation_Histamine signaling	8	3.8	1.5E-04	6.2E-03
Inflammation_Neutrophil activation	8	3.7	1.6E-04	6.2E-03
Inflammation_Innate inflammatoryresponse	7	3.9	3.3E-04	7.6E-03
Development_Neurogenesis_Synaptogenesis	7	3.9	3.3E-04	7.6E-03
Muscle contraction	6	3.5	1.7E-03	2.8E-02
Cell adhesion_Platelet-endothelium-leucocyte interactions	6	3.4	1.7E-03	2.8E-02
Transport_Potassium transport	6	3.1	3.0E-03	3.8E-02
Muscle contraction_Relaxin signaling	4	4.9	3.1E-03	3.8E-02
Immune response_Innate immune response to RNA viral infection	4	4.8	3.4E-03	3.8E-02

Performed using the Metacore software package.

Extended Data Table 4 | Laminin-derived peptides

Abbreviation	Sequence
AG73	Ac-NQEQVSPLRKRLQVQLSIRT-NH2
AG10	Ac-NQEQVSPLNRWHSIYITRFG-NH2
AG32	Ac-NQEQVSPLTWYKIAFQRNRK-NH2
A10	Ac-NQEQVSPLGTNNWWQSPSIQN-NH2
A13	Ac-NQEQVSPLRQVFQVAYIIIKA-NH2
A55	Ac-NQEQVSPLGGFLKYTVSYDI-NH2
A64	Ac-NQEQVSPLRDQLMTVLANVT-NH2
A2G80	Ac-NQEQVSPLVQLRNGFPYFSY-NH2
A203	Ac-NQEQVSPLMEMQANLLLDRL-NH2
A208	Ac-NQEQVSPLAASIKVAVSADR-NH2
A99	Ac-NQEQVSPLAGTFALRGDNPQG-NH2
EF1zz	Ac-NQEQVSPLATLQLQEGRLHF(Nle)FDLGKGR-NH2
bis-Cys AG73	Ac-GCRERKRLQVQLSIRTERCG-NH2

See refs 33, 34.